Journal of Mines, Metals and Fuels, *71(12B) : 252-260; 2023. DOI: 10.18311/jmmf/2023/45590*

Print ISSN : 0022-2755

Journal of Mines, Metals and Fuels

Contents available at: *www.informaticsjournals.com/index.php/jmmf*

Multiquadric Collocations for Nonlinear Vibration of Functionally Graded Plates of Ti–6Al–4V Metal

Pankaj Gupta[1*], Bhagat Singh[1], Yogesh Shrivastava[2] and Sunil Kumar[3]

[1]Jaypee University of Engineering and Technology, Mohanpur – 473226, Madhya Pradesh, India; pankaj.motivator@gmail.com

[2]Galgotias College of Engineering and Technology, Greater Noida – 201310, Uttar Pradesh, India

[3]GLA University, Chaumuhan – 281406, Uttar Pradesh, India

Abstract

While Finite Element Method (FEM) has proven reliable for analyzing linear or nonlinear stresses in materials, structures, and fluid flows, its reliance on mesh generation can escalate project simulation costs. In contrast, mesh- free techniques offer an alternative by directly generating system algebraic equations for the entire issue domain, bypassing the need for a preset mesh. This study focuses on investigating the nonlinear free vibration response of shear-deformable Functionally Graded Material (FGM) plates. These plates are expected to exhibit varying material properties, following a power-law distribution linked to the volume fractions of constituent materials as plate thickness increases. Utilizing shear deformation theories and von Karman nonlinear kinematics, the study seeks a mathematical solution for the real physical issues encountered in these plates. To address these challenges, a meshless method employing the Multi Quadric Radial Basis Function (MQRBF) is employed for evaluation. The computed results reveal insights into how different material properties and amplitudes influence the nonlinear free vibration response of composite plates. Comparing these outcomes to prior research demonstrates promising progress in this area.

Keywords: *FGM, Meshfree Method, MQRBF, Nonlinear Free Vibration, Plates*

1.0 Introduction

Harmonically stimulating rectangular plates composed of Functionally Graded Materials (FGM) is a common practice in ensuring the safety of building structures. Given the increasing use of high-performance structures across various industries, there's a pressing need for novel numerical techniques to accurately analyze them. While finite element and finite difference methods have been widely employed, meshless approaches have garnered significant attention in the past decade due to their ability to generate finite-dimensional subspaces with versatility.

Traditionally, meshless methods utilizing Radial Basis Functions (RBFs) have focused on approximating scattered data[1], but there's been a recent surge in interest in leveraging these techniques for solving Partial Differential Equations (PDEs) directly, offering a promising avenue for more efficient solutions. Meshfree analysis of composites has also become a focal point, with studies exploring various numerical methods for solving PDEs using RBFs[2,3].

For instance, Kansa's solution utilizes an asymmetrical RBF collocation method based on Multiquadric (MQ) interpolation functions[4], demonstrating the potential of RBFs in computational mechanics. Additionally, researchers have investigated meshless techniques for analyzing laminated plating, linear flexural and free vibration analysis of sandwich

**Author for correspondence*

and laminated composite plates[5], and studying buckling phenomena using wavelets and Wendland radial basis functions[6,7].

Recent studies have also delved into the buckling and bending behavior of isotropic skew and circular plates using moving least-squares differential quadrature[8] and meshfree approaches with recurring kernel approximations[9,10]. Investigating thermal conditions, researchers have explored notable oscillations of sandwich plates with functionally graded material face sheets[11] and conducted semi-analytical studies on the nonlinear free and forced axisymmetric vibrations of thin circular FGM plates[12,13], incorporating Von Karman's nonlinearity and traditional laminated plate theory.

In this context, the present work employs multiquadric radial basis functions to investigate the nonlinear free vibration of FGM plates. The obtained outcomes, compared with various numerical and analytical methods from earlier literature, demonstrate satisfactory agreement, highlighting the effectiveness of the approach in understanding the complex behavior of these structures.

2.0 Meshfree Colocation Method

This study examines the nonlinear free vibration of FGM plates utilizing the multiquadric radial basis function within a meshfree method. As a preliminary step, it is imperative to validate the meshfree Element Free Galerkin (EFG) colocation technique and Meshless Local Petrov-Galerkin (MLPG) for structural elements before delving into the primary focus of the research. Subsequently, the study compares various meshfree approaches for both 1D and 2D cantilever beams.

2.1 Cantilever 1D Beam with Liner Body Force

A one-dimensional, unit-length bar is applied with a liner body force of size x. The displacement of the bar is set at the left end and free of traction at the right. Bar has a constant crass-section area of unit magnitude and an elastic modulus of E.

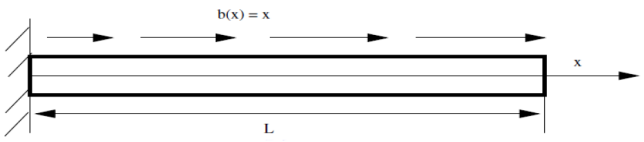


Figure 1. Using liner body force and cantilever 1D beam.

2.1.1 Meshfree EFG Method

Figure 2 depicts the compression of EFGM and the precise solution for α=3, whereas Figure 3 shows the same information for α=2.1.

Analyzing the effect of altering the Dimensionless Size of Support Domain on the nodal displacement parameter solution for the bar is quite easy. As a result, there is much disagreement about what constitutes an appropriate support domain size.

Our conclusion is that we should explore and try to lower the Dimensionless Size of Support Domain value before proceeding with the code. Additionally, we should check that the function's derivative and figure of

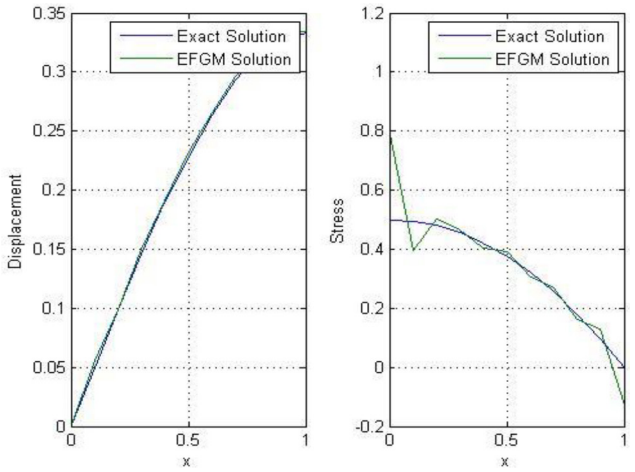


Figure 2. Displacement and stress for α=3.

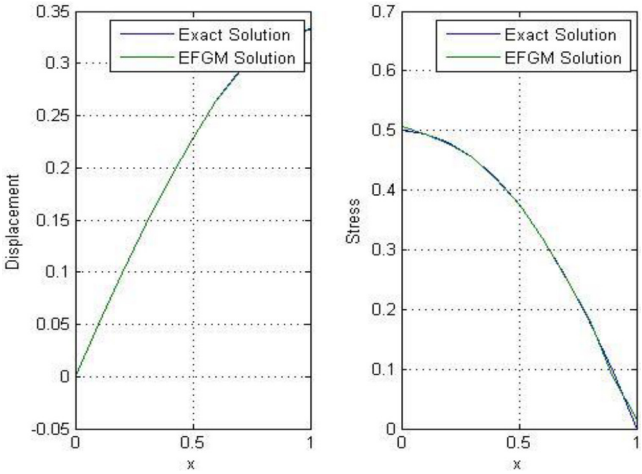


Figure 3. Displacement and stress for α=2.1.

the form function for each value seem organized and understandable.

2.2 Meshfree MLPG Approach

Figure 4 shows the Dimensionless Size of Support Domain, α=2.5, for α=2.1, Linear Basis, Cubic Spline weight function, Penalty method to enforce important boundary constraints, and MLS Approximation to generate Shape function.

2.3 Cantilever 2D Beam

As seen in Figure 5, a beam with dimensions W, T, unit depth, and plane tension condition is subjected to parabolic loading at one end. Timoshenko and Goodier provide a precise answer to this issue;

$$u_x = -\frac{P_y}{6EI}\left[(6W-3x)x+(2+\nu)(y^2-\frac{T^2}{4})\right] \quad 1$$

$$u_y = \frac{P}{6EI}\left[3\nu y^2(W-x)+(4+5\nu)\frac{T^2x}{4}+(3W-x)x^2\right] \quad 2$$

$$\sigma_x(x,y) = -\frac{P(W-x)y}{I} \quad 3$$

$$\sigma_y(x,y) = 0 \quad 4$$

$$\tau_{xy}(x,y) = -\frac{P_y}{2I}\left(\frac{T^2}{4}-y^2\right) \quad 5$$

where, I is considered as moment of inertia, which equals $T^3/12$ as other dimension is unit. This problem is now addressed using several meshfree techniques and contrasted with the precise solution found by Timoshenko and Goodier.

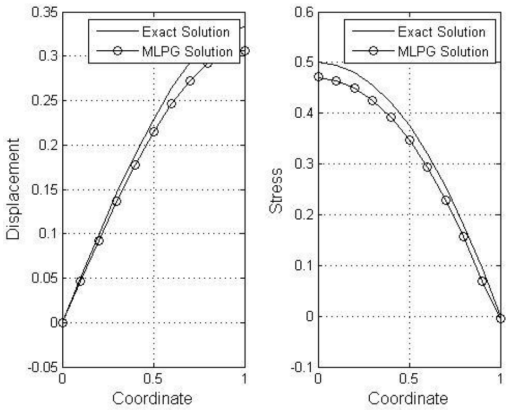


Figure 4. Displacement and stress for α=2.1.

2.3.1 *Meshfree EFG Collocation Method with Pattern Nodal Distribution*

Figure 6 illustrates the meshfree EFG collocation method with pattern nodal distribution. Lx=48, Ly=12, P=0.1, E=1, x=0.3, α=2.5, Liner basis function, and Cubic spline weight function are taken into consideration, as illustrated in Figure 7. The various stresses and deformations are compared to their precise values in these figures.

2.3.2 *Meshfree EFG Collocation Method with Random Nodal Distribution*

Figure 8 shows the meshfree EFG collocation method with random nodal distribution. Lx=48, Ly=12, P=0.1, E=1, x=0.3, α=2.5, Liner basis function, and Cubic spline weight function are taken into consideration, as illustrated in Figure 9. The various stresses and deformations are likewise compared to the precise values in these figures.

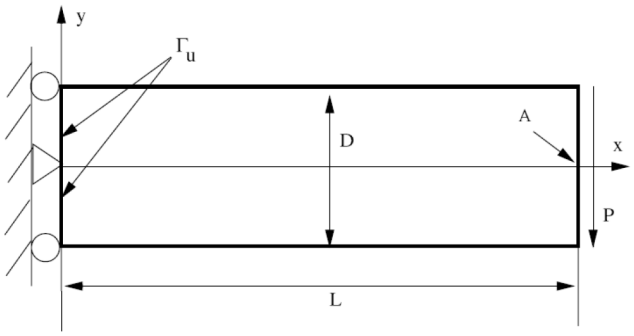


Figure 5. 2D cantilever beam.

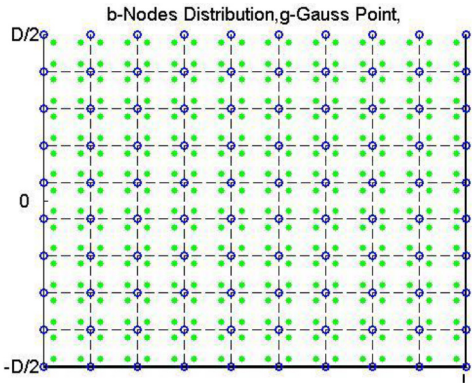


Figure 6. Meshfree EFG collocation method with pattern nodal distribution.

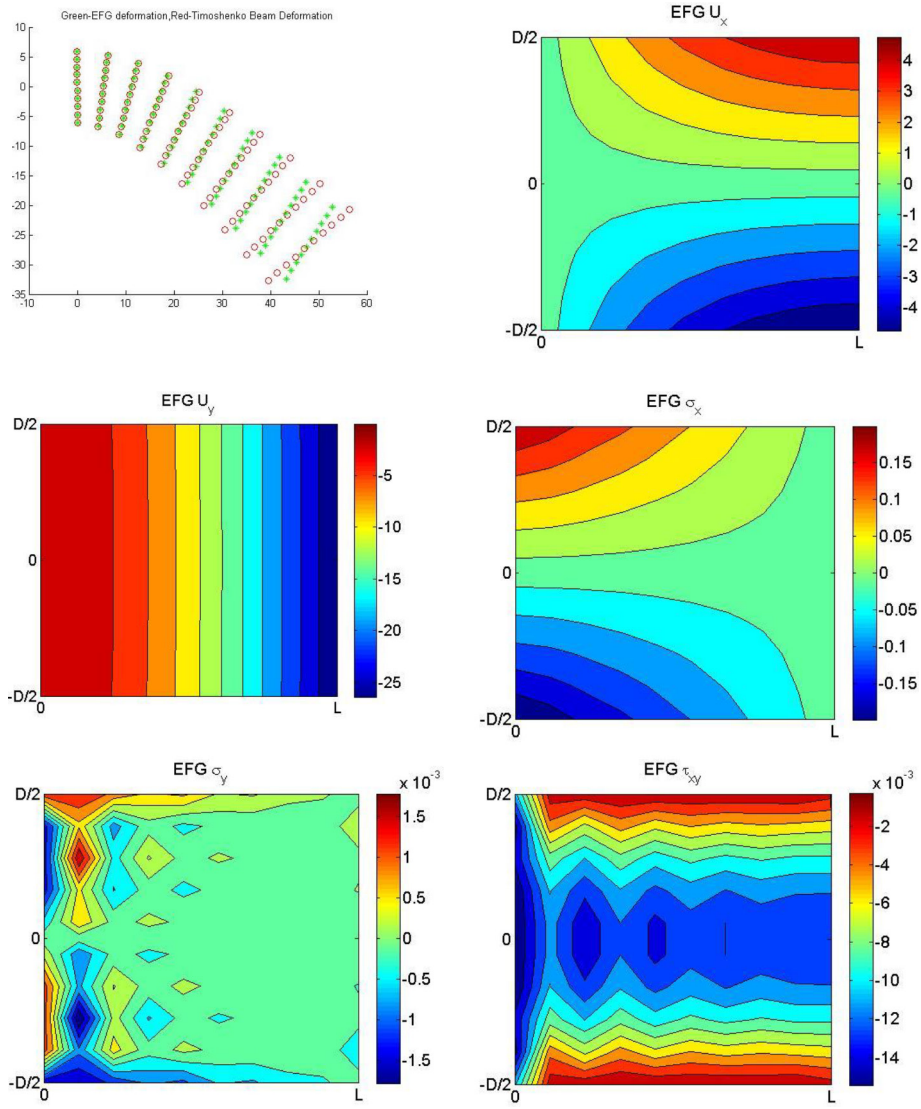


Figure 7. Comparison of results exact vs. meshfree and different deformations and stresses.

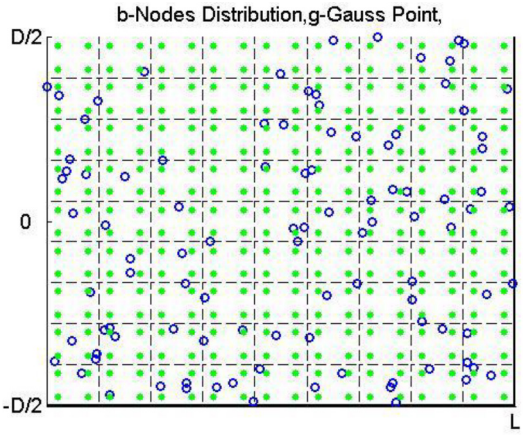


Figure 8. Meshfree EFG collocation method with random nodal distribution.

2.3.3 *Meshfree MLPG Collocation Method with Pattern Nodal Distribution*

Figure 10 illustrates the meshfree MLPG collocation method with pattern nodal distribution. Lx=48, Ly=12, P=0.1, E=1, x=0.3, α=2.5, Liner basis function, and Cubic spline weight function are taken into consideration, as illustrated in Figure 11. The various stresses and deformations are likewise compared to the precise values in these figures. The potential of meshfree EFG and MLPG collocation techniques is demonstrated in this section. After comparing the aforementioned analysis to Timoshenko and Goodier's precise solution, it can be concluded that the EFG collocation approach is a productive way to analyze structural materials. The

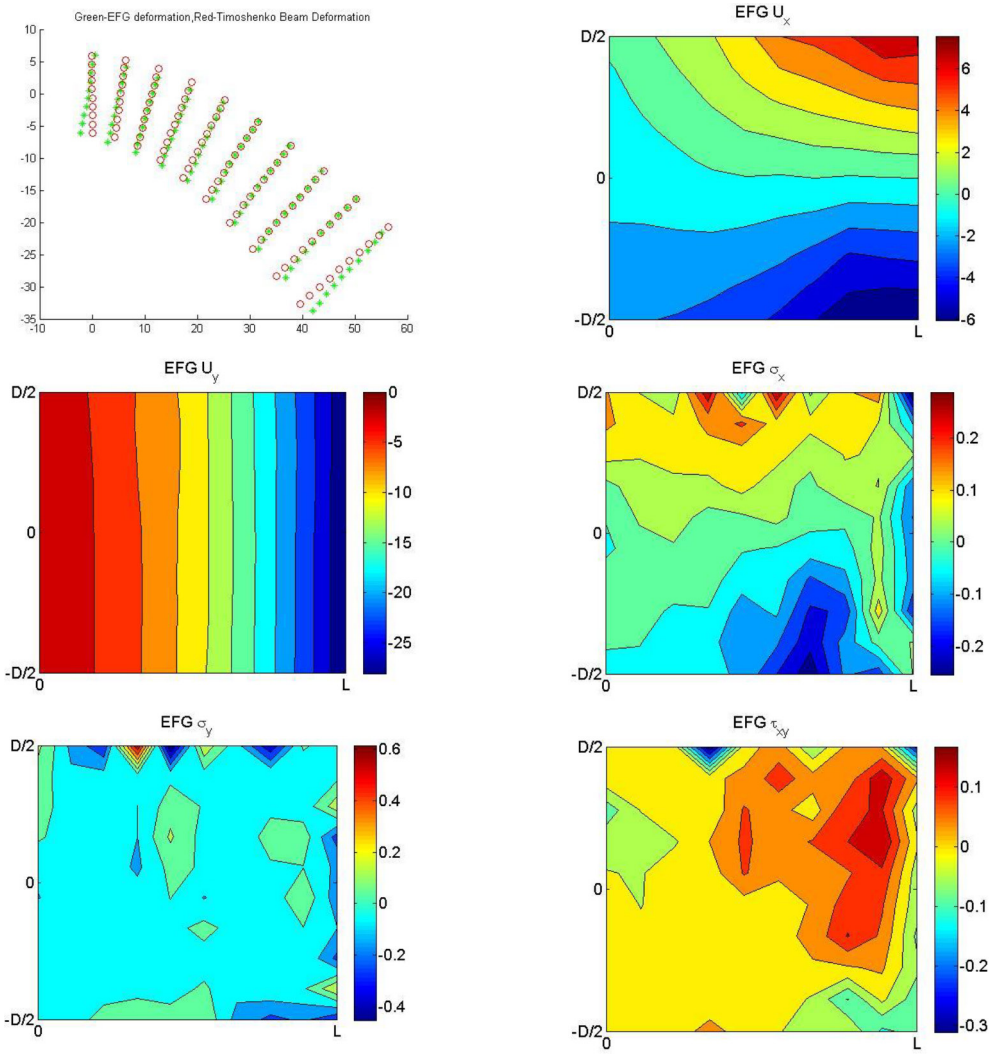


Figure 9. Comparison of results exact vs. meshfree and different deformations and stresses.

multiquadric radial basis function of meshfree approach is used in the next part to investigate the nonlinear free vibration of FGM plates.

3.0 Methodology

3.1 Governing Equations

With dimensions of "a" along the x-axis, "b" along the y-axis, and "h" along the z-axis, the object is a rectangular plate. The coordinate system's xy plane and the plate's midplane line up. It is anticipated that sandwich plates and laminated composites would attach perfectly. The displacement is as [13].

$$v = v_0 - z\frac{\partial w_0}{\partial y} + f(z)\phi_y \quad 6$$

$$u = u_0 - z\frac{\partial w_0}{\partial x} + f(z)\phi_x \quad 7$$

$$w = w_0 \quad 8$$

where the displacements of the plate in the transverse and in-plane directions at any given point (x, y, z, t) are indicated by the variables u, v, and w. At any position (x, y) where the plate's midpoint is positioned, the displacements in the x, y, and z directions are u0, v0, and w0, respectively. Functions φ_x and φ_y stand for the rotations of the midplane's normal caused by shear deformation around the x and y axes. The functions of transverse shear stress $f(z) = z\left(1 - \frac{4z^2}{3h^2}\right)$, introduced by Levinson[9]

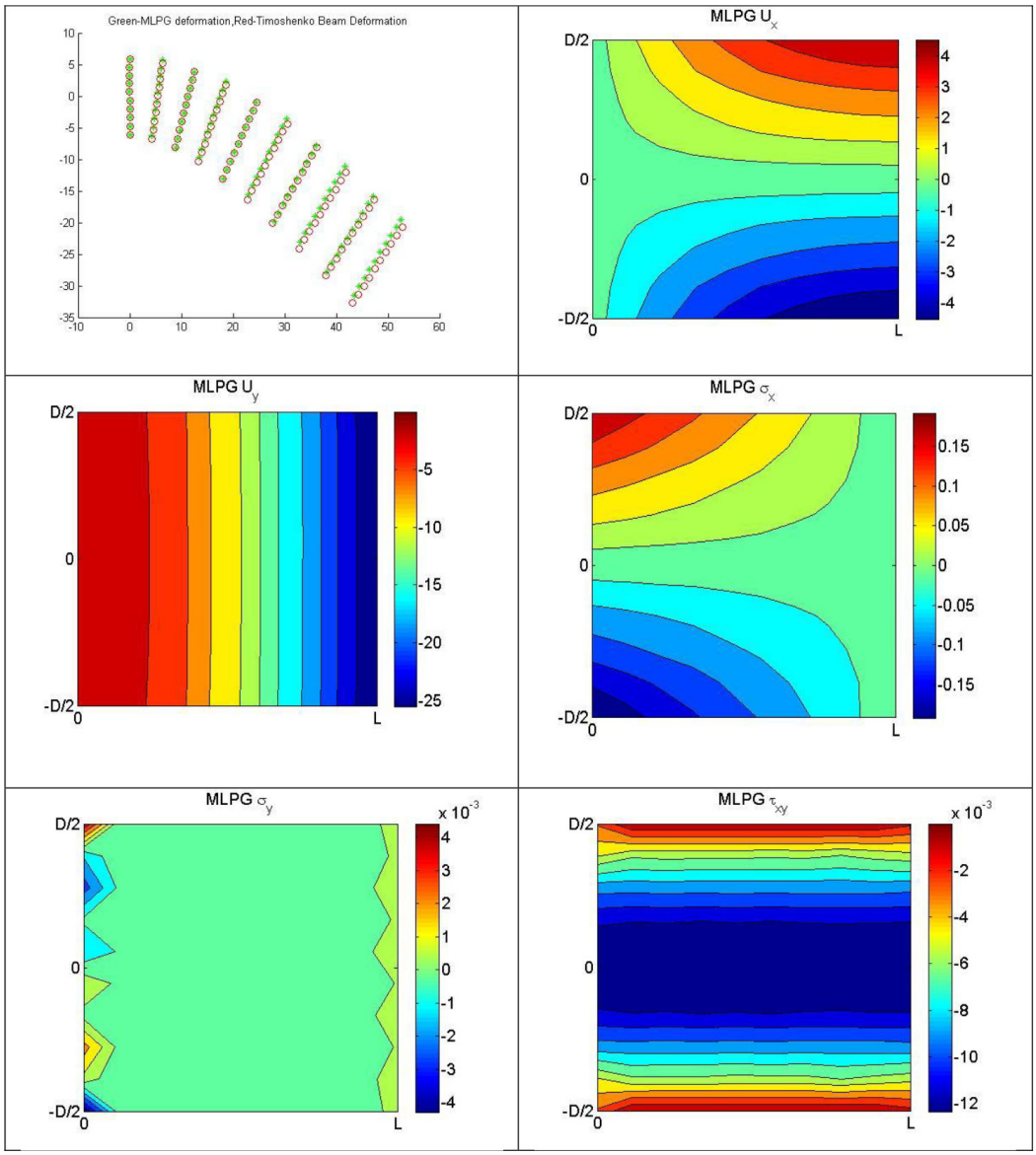


Figure 10. Meshfree MLPG collocation method with pattern nodal distribution.

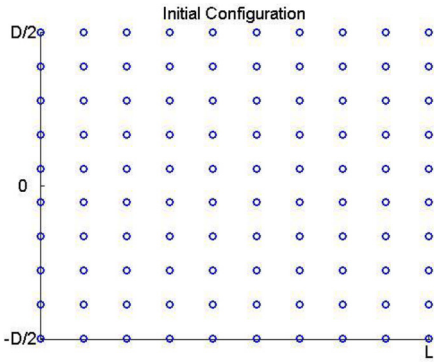


Figure 11. Comparison of results exact vs. meshfree and different deformations and stresses.

$$\begin{Bmatrix} \varepsilon_{xx} \\ \varepsilon_{yy} \\ \gamma_{xy} \end{Bmatrix} = \begin{Bmatrix} \dfrac{\partial u_0}{\partial x} - z\dfrac{\partial^2 w_0}{\partial x^2} + f(z)\dfrac{\partial \phi_x}{\partial x} + \dfrac{1}{2}\left(\dfrac{\partial w_0}{\partial x}\right)^2 \\ \dfrac{\partial v_0}{\partial y} - z\dfrac{\partial^2 w_0}{\partial y^2} + f(z)\dfrac{\partial \phi_y}{\partial y} + \dfrac{1}{2}\left(\dfrac{\partial w_0}{\partial y}\right)^2 \\ \dfrac{\partial u_0}{\partial y} + \dfrac{\partial v_0}{\partial x} - 2z\dfrac{\partial^2 w_0}{\partial x \partial y} + f(z)\dfrac{\partial \phi_x}{\partial y} \\ + f(z)\dfrac{\partial \phi_y}{\partial x} + \left(\dfrac{\partial w_0}{\partial x}\right)\left(\dfrac{\partial w_0}{\partial y}\right) \end{Bmatrix} \quad 9$$

$$\begin{Bmatrix}\gamma_{yz}\\ \gamma_{zx}\end{Bmatrix}=\begin{Bmatrix}\dfrac{\partial f(z)}{\partial z}\phi_y\\ \dfrac{\partial f(z)}{\partial z}\phi_x\end{Bmatrix} \quad 10$$

expressed as:

$$\delta u_0:\frac{\partial N_{xx}}{\partial x}+\frac{\partial N_{xy}}{\partial y}=\left(I_0\frac{\partial^2 u_0}{\partial \tau^2}-I_1\frac{\partial^3 w_0}{\partial x\partial \tau^2}+I_3\frac{\partial^2\phi_x}{\partial \tau^2}\right) \quad 11$$

$$\delta v_0:\frac{\delta N_{xy}}{\partial x}+\frac{\partial N_{yy}}{\partial y}=\left(I_0\frac{\partial^2 v_0}{\partial \tau^2}-I_1\frac{\partial^3 w_0}{\partial y\partial \tau^2}+I_3\frac{\partial^2\phi_y}{\partial \tau^2}\right) \quad 12$$

$$\delta w_0:\left(\frac{\partial N_{xx}}{\partial x}+\frac{\partial N_{xy}}{\partial y}\right)\left\{\frac{\partial w_o}{\partial x}\right\}+\left(\frac{\partial N_{yy}}{\partial y}+\frac{\partial N_{xy}}{\partial x}\right)\left\{\frac{\partial w_o}{\partial y}\right\}$$

$$+N_{xx}\frac{\partial^2 w_0}{\partial x^2}+N_{yy}\frac{\partial^2 w_0}{\partial y^2}+2N_{xy}\frac{\partial^2 w_0}{\partial x\partial y}$$

$$+\frac{\partial^2 M_{xx}}{\partial x^2}+\frac{\partial^2 M_{yy}}{\partial y^2}+2\frac{\partial^2 M_{xy}}{\partial x\partial y}-q_z$$

$$=I_0\frac{\partial^2 w_0}{\partial t^2}+I_1\left(\frac{\partial^3 u_0}{\partial x\partial \tau^2}+\frac{\partial^3 v_0}{\partial y\partial \tau^2}\right)-I_2\left(\frac{\partial^4 w_0}{\partial x^2\partial \tau^2}+\frac{\partial^4 w_0}{\partial y^2\partial \tau^2}\right)$$

$$+I_4\left(\frac{\partial^4\phi_x}{\partial x^2\partial \tau^2}+\frac{\partial^4\phi_y}{\partial y^2\partial \tau^2}\right) \quad 13$$

$$\delta\phi_x:\frac{\partial M^f_{xx}}{\partial x}+\frac{\partial M^f_{xy}}{\partial y}-Q^f_x=\left(I_3\frac{\partial^2 u_0}{\partial \tau^2}-I_4\frac{\partial^3 w_0}{\partial x\partial \tau^2}+I_5\frac{\partial^2\phi_x}{\partial \tau^2}\right) \quad 14$$

$$\delta\phi_y:\frac{\partial M^f_{xy}}{\partial x}+\frac{\partial M^f_{yy}}{\partial y}-Q^f_y=\left(I_3\frac{\partial^2 v_0}{\partial \tau^2}-I_4\frac{\partial^3 w_0}{\partial y\partial \tau^2}+I_5\frac{\partial^2\phi_y}{\partial \tau^2}\right) \quad 15$$

An equation for the force, moment, and stiffness coefficients in the plate is given by Singh and Shukla[14].
Clamped:

$$x=0,a:u_0=0,w_0=0,\phi_x=0,N_{xy}=0,\phi_y=0 \quad 16$$

$$y=0,b:v_0=0,w_0=0,N_{xy}=0,\phi_x=0,\phi_y=0 \quad 17$$

Simply supported:

$$x=0,a:v_0=0,w_0=0\,N_{xx}=0,M_{xx}=0,\phi_y=0 \quad 18$$

$$y=0,b:u_0=0,w_0=0,\phi_x=0,N_{yy}=0,M_{yy}=0 \quad 19$$

4.0 Results and Discussions

For the analyses, a square FGM plate with the following material characteristics is used: Titanium alloy (Ti–6Al–4V: metal) $E = 105.7ttPa$, ν = 0.298, $\rho = 4429kg/m^3$

Zirconia (ZrO_2: ceramic) $E = 200ttPa$, $\nu = 0.3$, $\rho = 3000kg/m^3$ resents the results of frequency ratio (ω_nl/ω_l) and FEM results from Talha and Singh[15].

A study was carried out to show how the frequency ratio of simply supported square zirconium oxide (ZrO_2) and titanium alloy (Ti–6AL–4V) Functionally

Table 1. Comparing the results for FGM plate

Source	(W_max/h)				
	0.2	**0.4**	**0.6**	**0.8**	**1**
current work (7x7)	1.0568	1.1338	1.2685	1.4155	1.5955
current work (9x9)	1.0502	1.1376	1.2729	1.4203	1.6009
current work (11x11)	1.0472	1.1388	1.2742	1.4218	1.6026
current work (13x13)	1.0453	1.1411	1.2767	1.4247	1.6058
Talha work[15] (5x5)	1.0455	1.1409	1.2765	1.4244	1.6055
Huang work[16]	1.021	1.082	1.176	1.296	1.436

Table 2. Impact of amplitude ratio and volume fraction in FGM plate

n	(W_max/h)							
	0.5	0.5	1	1	2	2	3	3
	current work	Talha work[15]	current work	Talha work[15]	current work	Talha work[15]	current work	Talha work[15]
0	1.2127	1.2144	1.7162	1.6953	2.3832	2.2563	3.5402	3.2223
0.2	1.1972	1.1989	1.6467	1.6266	2.2824	2.1609	2.7284	2.4834
0.4	1.1596	1.1613	1.6195	1.5997	2.2744	2.1533	2.4197	2.2024
0.6	1.1390	1.1406	1.5952	1.5757	2.2030	2.0857	2.4248	2.2071
0.8	1.0611	1.0626	1.5629	1.5438	2.1212	2.0083	2.4009	2.1853
1.0	1.1234	1.1250	1.5517	1.5328	2.0455	1.9366	2.2442	2.0427

The frequency ratio rises in proportion to an increase in the amplitude ratio. Volume fraction increases, the rigidity decreases.

Table 3. FGM plate as a function of amplitude ration and thickness ratio

a/h	(W_max/h) 0.5	0.5	1	1	2	2
	Current work	Talha work[15]	Current work	Talha work[15]	Current work	Talha work[15]
15	1.4178	1.4192	1.5856	1.6088	2.3459	2.3801
25	1.3064	1.3077	1.5835	1.6066	2.0835	2.1139
50	1.2102	1.2114	1.5397	1.5622	2.0916	2.1221
100	1.2068	1.2080	1.4736	1.4951	1.8802	1.9076

Graded Material (FGM) plates is affected by the volume fraction index 'n'. The plate's bottom surface is metal-rich (Ti-6AL-4V) while its top surface is ceramic-rich (ZrO_2). Table 2 presents and validates the results in conjunction with Talha and Singh's FEM findings[15].

The frequency ratio rises in proportion to an increase in the amplitude ratio. Volume fraction increases, the rigidity decreases.

Table 3 shows how a square SSSS FGM plate (n=1)'s (ω_nl/ω_l) is affected by amplitude ratio and thickness ratio[15,16]. The validity of the procedure is satisfactory as shown in comparison table. The plate's span thickness ratio falls, frequency ratio rises.

5.0 Conclusion

The study presents nonlinear free vibration responses of rectangular FGM plates under various boundary conditions. Prior to the investigation, the accuracy and suitability of the meshless technique for colocation were verified. The study then compares the precise responses obtained using Meshfree EFG and Meshfree MLPG approaches for both 1D and 2D cases. Structural component analysis demonstrated the efficacy of the EFG collocation approach. Initially, a finite element approach was employed to analyze a rectangular FGM plate. Subsequently, the study contrasted the results obtained using finite element analysis with those obtained using the multiquadric RBF-based previous analytical and numerical findings.

6.0 References

1. Kumar M, Jha AK, Bhagoria Y, Gupta P. A review to explore different meshless methods in various structural problems. IOP Conf Ser Mater Sci Eng. 2021; 1116(1):012119. https://doi.org/10.1088/1757-899X/1116/1/012119
2. Liew KM, Zhao X, Ferreira AG. A review of meshless methods for laminated and functionally graded plates and shells. Compos Struct. 2011; 93(8):2031-41. https://doi.org/10.1016/j.compstruct.2011.02.018
3. Kumar R, Lal A, Singh BN, Singh J. New transverse shear deformation theory for bending analysis of FGM plate under patch load. Compos Struct. 2019; 208:91-100. https://doi.org/10.1016/j.compstruct.2018.10.014
4. Pham QH, Nguyen PC, Tran TT. Free vibration response of auxetic honeycomb sandwich plates using an improved higher-order ES-MITC3 element and artificial neural network. Thin-Walled Struct. 2022; 175:109203-3. https://doi.org/10.1016/j.tws.2022.109203
5. Huang J, Nguyen-Thanh N, Gao J, Fan Z, Zhou K. Static, free vibration, and buckling analyses of lami-

nated composite plates via an isogeometric meshfree collocation approach. Compos Struct. 2022; 285:115011. https://doi.org/10.1016/j.compstruct.2021.115011
6. Ferreira M, Castro LM, Roque C, Reddy JN, Bertoluzza S. Buckling analysis of laminated plates by wavelets. Comput Struct. 2011; 89(7-8):626-30. https://doi.org/10.1016/j.compstruc.2011.01.007
7. Ferreira AJM, Roque CMC, Neves AMA, Jorge RMN, Soares CMM, Liew KM. Buckling and vibration analysis of isotropic and laminated plates by radial basis functions. Compos Part B Eng. 2011; 42(3):592-606. https://doi.org/10.1016/j.compositesb.2010.08.001
8. Kharghani N, Soares CG. Experimental, numerical and analytical study of buckling of rectangular composite laminates. Eur J Mech - A/Solids. 2020; 79:103869–9. https://doi.org/10.1016/j.euromechsol.2019.103869
9. Liew KM, Wang J, Ng TY, Tan MJ. Free vibration and buckling analyses of shear-deformable plates based on FSDT meshfree method. J Sound Vib. 2004; 276(3-5):997-1017. https://doi.org/10.1016/j.jsv.2003.08.026
10. Maithil P, Gupta P, Chandravanshi ML. Study of mechanical properties of the natural-synthetic fiber reinforced polymer matrix composite. Today Proc. 2023. https://doi.org/10.1016/j.matpr.2023.01.245
11. Vasara D, Khare S, Sharma HK, Kumar R. Free vibration analysis of functionally graded porous circular and annular plates using differential quadrature method. Forces Mech. 2022; 9:100126. https://doi.org/10.1016/j.finmec.2022.100126
12. Allahverdizadeh A, Naei MH, Bahrami MN. Nonlinear free and forced vibration analysis of thin circular functionally graded plates. J Sound Vib. 2008; 310(4-5):966-84. https://doi.org/10.1016/j.jsv.2007.08.011
13. Liew KM, Chen XL, Reddy JN. Mesh-free radial basis function method for buckling analysis of non-uniformly loaded arbitrarily shaped shear deformable plates. Comput Methods Appl Mech Eng. 2004; 193(3-5):205-24. https://doi.org/10.1016/j.cma.2003.10.002
14. Singh J, Shukla KK. Nonlinear flexural analysis of functionally graded plates under different loadings using RBF based meshless method. Eng Anal Bound Elem. 2012; 36(12):1819-27. https://doi.org/10.1016/j.enganabound.2012.07.001
15. Talha M, Singh BN. Large amplitude free flexural vibration analysis of shear deformable FGM plates using nonlinear finite element method. Finite Elem Anal Des. 2011; 47(4):394-401. https://doi.org/10.1016/j.finel.2010.11.006
16. Trinh MC, Nguyen DD, Kim SE. Effects of porosity and thermomechanical loading on free vibration and nonlinear dynamic response of functionally graded sandwich shells with double curvature. Aerosp Sci Technol, 2019; 87:119-32. https://doi.org/10.1016/j.ast.2019.02.010